The Dynamic Compressive Response of Open-Cell Foam Impregnated With a Newtonian Fluid

M. A. Dawson
e-mail: dawson@mit.edu

G. H. McKinley

Department of Mechanical Engineering,
Massachusetts Institute of Technology,
Cambridge, MA 02139

L. J. Gibson
Department of Materials Science
and Engineering,
Massachusetts Institute of Technology,
Cambridge, MA 02139

This analysis considers the flow of a highly viscous Newtonian fluid in a reticulated, elastomeric foam undergoing dynamic compression. A comprehensive model for the additional contribution of viscous Newtonian flow to the dynamic response of a reticulated, fluid-filled, elastomeric foam under dynamic loading is developed. For highly viscous Newtonian fluids, the flow in the reticulated foam is assumed to be dominated by viscous forces for nearly all achievable strain rates; Darcy's law is assumed to govern the flow. The model is applicable for strains up to the densified strain for all grades of low-density, open-cell, elastomeric foam. Low-density, reticulated foam is known to deform linear elastically and uniformly up to the elastic buckling strain. For strains greater than the elastic buckling strain but less than the densified strain, the foam exhibits bimodal behavior with both linear-elastic and densified regimes. The model presented in this analysis is applicable for all strains up to the densified strain. In the bimodal regime, the model is developed by formulating a boundary value problem for the appropriate Laplace problem that is obtained directly from Darcy's law. The resulting analytical model is more tractable than previous models. The model is compared with experimental results for the stress-strain response of low-density polyurethane foam filled with glycerol under dynamic compression. The model describes the data for foam grades varying from 70 ppi to 90 ppi and strain rates varying from 2.5×10^{-3} to 10^{1} s^{-1} well. The full model can also be well approximated by a simpler model, based on the lubrication approximation, which is applicable to analyses where the dimension of the foam in the direction of fluid flow (radial) is much greater than the dimension of the foam in the direction of loading (axial). The boundary value model is found to rapidly converge to the lubrication model in the limit of increasing aspect ratio given by the ratio of the radius R, to the height h, of the foam specimen with negligible error for aspect ratios greater than $R/h \sim 4$. [DOI: 10.1115/1.2912940]

Keywords: boundary value problem, fluid-structure interaction, foam, lubrication approximation, porous media

1 Introduction

Over the past century, much of the research in developing armor has focused on providing protection against ballistics. This research has culminated in highly advanced armor for defending against projectiles [1]; however, existing armor is inefficient at protecting against the enormous pressure gradients generated by explosive devices. These blast waves can cause severe damage to the human body as well as vehicles and structures. Recently, a novel reactive armor design to mitigate the effects of blast waves has been explored [2]. This design incorporates open-cell (reticulated) foams filled with shear thickening, non-Newtonian liquids into existing composite armor. Open-cell foams filled with non-Newtonian liquids have the potential to absorb energy and impede shock waves, which decrease the resulting pressure gradient experienced by underlying media (e.g., tissue). As a first step in modeling this nonlinear phenomenon, we analyze the flow of a Newtonian fluid through an open-cell, elastomeric foam. The flow of fluids through open-cell foams has been investigated extensively for a variety of engineering applications, but characterizing the contribution of the fluid to energy absorption under dynamic loading is still a critical area of research. Previous research has resulted in the development of complex models to describe the contribution of Newtonian fluids in an open-cell foam under impact loading. Hilyard [3] provided one of the first and only in-depth analytical and experimental analyses of the contribution of fluid flow to the impact behavior of open-cell foams, developing a third order, nonlinear equation of motion. Rehkopf, et al. [4], Mills and Lyn [5], and Schraad and Harlow [6] all developed finite difference and finite volume techniques to analyze the contribution of the fluid flow in an open-cell foam under dynamic loading. However, the inherent complexity of these models has limited their use.

In this paper, we develop a tractable but comprehensive analytical model for the additional contribution of viscous Newtonian flow to the stress-strain response of low-density, reticulated, fluid-filled, elastomeric foams under dynamic loading. Elastomeric foams deform in a linear-elastic manner, primarily by cell wall bending at strains below the elastic buckling strain. At strains between the elastic buckling strain and the densified strain, local bands of cells collapse, so that the foam has both a linear-elastic regime and a densified regime. As the overall strain increases, the densified regime expands at the expense of the linear-elastic regime [7]. We consider a model, which governs both the single regime and the bimodal regime of the fluid-filled foam. The prob-

Contributed by the Applied Mechanics Division of ASME for publication in the JOURNAL OF APPLIED MECHANICS. Manuscript received May 18, 2007; final manuscript received February 14, 2008; published online May 14, 2008. Review conducted by Nesreen Ghaddar.

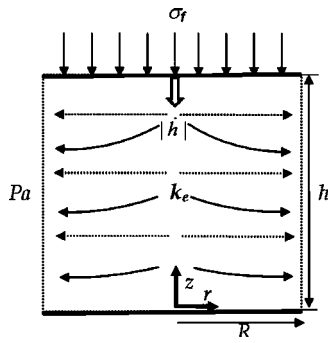

Fig. 1 One-regime model of fluid-filled cylindrical foam with strain less than the elastic buckling strain, $\varepsilon < \varepsilon^*_{el}$. Velocity of fluid (solid arrow). Relative velocity of fluid with respect to the velocity of foam (dotted arrow).

lem considers the axial compression of a cylindrical specimen of low-density, elastomeric foam filled with a highly viscous Newtonian fluid between a fixed plate and a moving plate (Figs. 1 and 2). Based on the low values of the characteristic Reynolds number in the pores, the flow of viscous Newtonian fluids in porous media is dominated by viscous forces for nearly all achievable strain rates; therefore, Darcy's law is assumed to govern the flow. Darcy's law is selected instead of the slightly more complicated Brinkman–Darcy model, which incorporates both a viscous contribution and an additional term, attributed primarily to the inertial forces dominant in the high Reynold's number regime (Dawson et al. [7]). For the more complex bimodal regime problem, Darcy's law is used to formulate a boundary value problem with Laplace's equation as the governing differential equation. The solution to Laplace's equation in cylindrical coordinates for the pressure distribution in the fluid is formulated in terms of an infinite series of Bessel functions. The solution rapidly converges within the first few terms and is readily evaluated numerically. The pressure distribution is used to find a model for the contribution of the fluid to the stress-strain response of the fluid-filled foam.

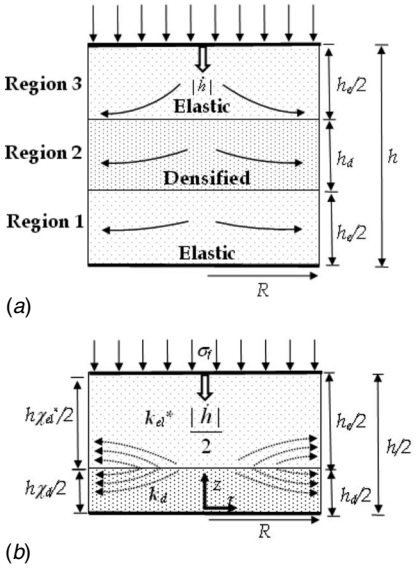

Fig. 2 (*a*) Bimodal regime model of fluid-filled cylindrical foam compressed beyond elastic buckling strain, $\varepsilon^*_{el} < \varepsilon < \varepsilon_d$. Velocity of fluid. (solid arrow) (*b*). Top symmetric half of bimodal regime model of fluid-filled cylindrical foam compressed beyond elastic buckling strain, $\varepsilon^*_{el} < \varepsilon < \varepsilon_d$, in the reference frame of the densified regime. Relative velocity of fluid with respect to the velocity of foam (dotted arrow).

The model is analytically tractable and applicable for strains up to the densified strain for all grades of low-density, flexible, open-cell foam. We also develop a more simple model based on the lubrication approximation to approximate the more comprehensive boundary value model in the limit where the characteristic dimension in the direction of fluid flow (radial) is assumed to be much greater than that in the direction of loading (axial). The rapid convergence of the boundary value model toward the lubrication, as the aspect ratio is increased, is discussed. The model is also compared with experimental results of the stress-strain response of low-density polyurethane foam filled with glycerol under dynamic loading. The model gives a good description of the experimental results for foam grades varying from 70 ppi to 90 ppi and for strain rates varying from 2.5×10^{-3} to 10^1 s^{-1}. The model in this paper is not compared to previous models found in literature because comparable models with the ability to characterize the stress response necessitate extensive computational effort and would require dedicating a large portion of the paper to simply review the models and their applicability.

2 Literature Review

2.1 Stress-Strain Response of Foam. Gibson and Ashby [8] previously developed a model for the compressive stress-strain response of reticulated foam, neglecting any contribution of a viscous fluid. The governing equations are given by [8]

$$\sigma^* = \varepsilon E^*, \quad 0 < \varepsilon < \varepsilon^*_{el} \tag{1}$$

$$\sigma^* = \sigma^*_{el}, \quad \varepsilon^*_{el} < \varepsilon < \varepsilon_D\left(1 - \frac{1}{D}\right) + \varepsilon^*_{el} \tag{2}$$

$$\sigma^* = \frac{\sigma^*_{el}}{D}\left(\frac{\varepsilon_D}{\varepsilon_D - \varepsilon}\right)^m, \quad \varepsilon > \varepsilon_D\left(1 - \frac{1}{D}\right) + \varepsilon^*_{el} \tag{3}$$

where $\sigma^\star$ is the average, uniform stress response of the foam or the axial compressive force divided by the cross-sectional area of the foam, $E^\star$ is the effective modulus of the foam, ε is the strain, taken to be positive in compression and given by the compression deformation of the foam over the initial height of the foam, ε^*_{el} is the elastic buckling strain, σ^*_{el} is the elastic buckling stress, and m and D are constants associated with the microstructure of the foam. For polyurethane foams, Gibson and Ashby [8] gave the constant m as unity. The fully densified strain ε_D is the strain at which point the cells have collapsed sufficiently that opposing cell walls touch and further deformation compresses the cell wall material itself. The densified strain is given by

$$\varepsilon_D = 1 - 1.4\left(\frac{\rho^*_0}{\rho_s}\right) \tag{4}$$

where ρ^*_0 is the initial density of the foam at zero strain, and ρ_s is the density of the solid from which the foam is made. The constant D is given by

$$D = \frac{\varepsilon_D}{\varepsilon_D - \varepsilon^*_p} \tag{5}$$

where the strain ε^*_p corresponds to the strain at which the stress at the end of the plateau region begins to exceed the elastic buckling stress.

2.2 Microstructural Behavior of Foam Under Deformation. We utilize the model for the microstructural behavior of low-density, reticulated foam under compressive strain presented by Dawson et al. [7]. The cells of the foam under compressive strain remain elastic up to the linear-elastic buckling strain (Fig. 1). As the foam is compressed beyond the elastic buckling

strain, cells buckle and collapse without laterally expanding so that Poisson's ratio in this regime is approximately zero. These collapsed regions generate local bands of large deformation in which the average diameter of the cells is reduced substantially. The strain of the collapsed cells in these densified bands is assumed to be uniform and given by the densified strain ε_d, while the cells outside the densified bands remain in the linear elastic regime, at strains given by the elastic buckling strain (Fig. 2). Therefore, for strains less than the elastic buckling strain, the entire specimen is assumed to be uniform and completely within the linear-elastic regime, which results in a single regime problem. For strains greater than the elastic buckling strain but less than the densified strain, the foam is assumed to be a two-regime problem with both a linear-elastic region and a densified region (Fig. 2). Dawson et al. [7] used visual imaging to establish the value of the densified strain $\varepsilon_d=0.6$, for low-density, reticulated polyurethane foam. It is important to distinguish the densified strain ε_d from the fully densified strain ε_D given by Eq. (4), where the former effectively represents the onset of the densification regime, and the latter effectively represents the end of the densification regime.

At any given strain, the volume fractions of the cells remaining in the linear-elastic regime χ^*_{el} and the densified regime χ_d are given by [7]

$$\chi^*_{\text{el}} = \frac{(\varepsilon_d - \varepsilon)(1+\varepsilon^*_{\text{el}})}{(1+\varepsilon)(\varepsilon_d - \varepsilon^*_{\text{el}})} \tag{6}$$

$$\chi_d = \frac{(\varepsilon - \varepsilon^*_{\text{el}})(1+\varepsilon_d)}{(1+\varepsilon)(\varepsilon_d - \varepsilon^*_{\text{el}})} \tag{7}$$

After the densified strain is exceeded, cells begin to densify further, and this model is no longer applicable. Based on this model, Dawson et al. developed equations for the local permeability of open-cell foams in the linear-elastic regime, k_e, at the elastic buckling strain, k^*_{el}, and at the densified strain, k_d, which are given by [7]

$$k_e = A d_0^2 (1-\varepsilon)\left(1 - \frac{\rho^*_0}{\rho_s}\frac{1}{(1-\varepsilon)}\right)^3 \quad \text{for } 0 \le \varepsilon \le \varepsilon^*_{\text{el}} \tag{8}$$

$$k^*_{\text{el}} = A d_0^2 (1-\varepsilon^*_{\text{el}})\left(1 - \frac{\rho^*_0}{\rho_s}\frac{1}{(1-\varepsilon^*_{\text{el}})}\right)^3 \quad \text{for } \varepsilon = \varepsilon^*_{\text{el}} \tag{9}$$

$$k_d = A d_0^2 (1-\varepsilon_d)^{2a}\left(1 - \frac{\rho^*_0}{\rho_s}\frac{1}{(1-\varepsilon_d)}\right)^3 \quad \text{for } \varepsilon = \varepsilon_d \tag{10}$$

where d_0 is the average pore diameter at zero strain, and A is an empirical constant given by Brace [9] as 0.025 for a porous microstructure consisting of tubes with circular cross sections. The material properties of the foam, ρ^*_0, ρ_s, and d_0, are readily available and typically specified by the manufacturer. Dawson et al. [7] also found that these models are independent of the fluid flow direction with respect to the compression direction of the foam.

2.3 Flow in Porous Media. The flow of highly viscous Newtonian fluids in low-density, open-cell foam with small cell sizes (typically less than 500 μm) is dominated by viscous forces for nearly all achievable strain rates. Therefore, the model presented in this paper only considers flows in which the viscous effects dominate the inertial effects. The Reynolds number Re, a measure of the inertial forces to the viscous forces, can be used to determine where this model is applicable. A characteristic pore Reynolds number based on the average diameter of a pore, d, and average velocity through that pore, v, is given by

$$\text{Re} = \frac{\rho v d}{\mu} \tag{11}$$

where ρ is the density of the fluid and μ is the viscosity of the fluid. Based on an analytical study, Comiti et al. [10] proposed a transition from the viscous dominated regime to the inertial dominated regime at a critical pore Reynolds number of $\text{Re}^*=0.83$ for flow through low-density, porous media. This corresponds well with the experimental findings of Gent and Rusch [11] for flow through reticulated foam, Tek [12] for flow through porous rock, and Dybbs and Edwards [13] for flow through fixed beds of spheres and cylinders. Therefore, the model presented in this analysis is taken to be applicable for $\text{Re} \ll 1$ when viscous forces dominate. Based on a transition number of $\text{Re} \approx 1$, the maximum strain rate for which this analysis accurately models the flow of a highly viscous fluid in an open-cell foam can be determined. The experimental results presented below consist of a dynamic compression glycerol-filled, reticulated foam with an approximate radius and average cell diameter of 12.7 mm and 235 μm, respectively. At 23 °C, the density and viscosity of glycerol are taken to be $\rho=1260$ kg/m^3 and $\mu=1.1$ Pa s, respectively. The maximum strain rate for which the flow will remain in the viscous regime is found to be approximately 600 s^{-1}. The maximum strain rate of the foam specimens in the experiments presented is 10 s^{-1}, which thus lies well within the viscous dominated regime.

3 Analysis

3.1 Fluid Contribution to the Stress-Strain Response. A comprehensive model for the contribution of the fluid to the stress-strain response of fluid-filled, elastomeric foam under dynamic compression can be developed by extending the model presented by Dawson et al. [7]. We consider the case of axial compression of a cylindrical foam specimen where the lower plate is fixed and the upper plate is moving with the magnitude of the velocity given by $|\dot{h}|$, or the time rate of change of the height of the foam specimen, as shown in Figs. 1 and 2(*a*). The initial height and radius of the specimen are taken to be h_0 and R. As the foam undergoes compression, the radius of the specimen remains unchanged while the current height is given as $h(t)$. This analysis considers both the response at strains less than the elastic buckling strain and the response at strains greater than the elastic buckling strain but less than the densified strain. For strains less than the elastic buckling strain, the entire specimen is assumed to be uniform and completely within the linear-elastic regime, which results in a single regime problem (Fig. 1). For strains greater than the elastic buckling strain but less than the densified strain, the foam is assumed to coexist in two states with both a linear-elastic regime and a densified regime (Figs. 2(*a*) and 2(*b*)).

3.2 Single Regime Model $\varepsilon < \varepsilon^*_{\text{el}}$. We first consider the single regime problem with strain less than the elastic buckling strain. As the upper plate compresses the foam, the foam is assumed to deform uniformly. The relative velocity of the fluid with respect to the foam in the compression direction (z-direction) is taken to be zero throughout the foam. Any nonzero relative velocity in the z-direction would require flow up a pressure gradient in the radial direction, which violates Darcy's law. Therefore, neglecting gravitational effects, the pressure gradient throughout the foam in the z-direction is taken to be zero. Thus, the radial velocity of the fluid in the linear-elastic regime V_e is uniform in the z-direction and given as (after Gibson and Ashby [8])

$$V_e = \frac{-\dot{h} r}{2h\Phi}, \quad 0 \le \varepsilon \le \varepsilon^*_{\text{el}} \tag{12}$$

where Φ is the porosity of the foam, r is the radial distance, and h is the current height of the foam specimen, given by $h(t)=h_0(1-\varepsilon)$. According to Darcy's law, the gradient of the pressure across

the specimen $\partial P/\partial r$ for viscous Newtonian flow in the r-direction is given as [14]

$$\frac{\partial P}{\partial r} = \frac{-\mu V_e}{k_e}, \quad 0 \le \varepsilon \le \varepsilon_{\text{el}}^* \tag{13}$$

where μ is the dynamic viscosity of the fluid and the linear-elastic permeability k_e is taken to be isotropic. Combining Eqs. (12) and (13) and integrating give

$$P^* = \frac{\mu \dot{h}}{4\Phi h k_e}(r^2 - R^2), \quad 0 \le \varepsilon \le \varepsilon_{\text{el}}^* \tag{14}$$

where P^* is the local pressure minus the atmospheric pressure at the free surface of the foam. Neglecting inertial effects, a force balance can be used to find an equivalent average uniform stress distribution σ_f applied by the fluid to the top compression plate by integrating the pressure field over the radius giving

$$\sigma_f \pi R^2 = \int_0^R P^*|_h 2\pi r dr, \quad 0 \le \varepsilon \le \varepsilon_{\text{el}}^* \tag{15a}$$

$$\sigma_f = \frac{-\mu \dot{h} R^2}{8\Phi h k_e}, \quad 0 \le \varepsilon \le \varepsilon_{\text{el}}^* \tag{15b}$$

3.3 Bimodal Regime Model $\varepsilon_{\text{el}}^* < \varepsilon < \varepsilon_d$. For strains beyond the elastic buckling strain but less than the densified strain, the cells of the foam are assumed to be either at the elastic buckling strain or at the densified strain, corresponding to the bimodal regime model previously discussed. The resulting pressure distribution in both regimes is more complex than in the single regime problem and can be solved by means of coupling two boundary value problems. In formulating the boundary conditions for this problem, a model for the behavior of the foam must be developed. Under axial compression, densified bands are commonly observed to initiate in the center of the sample. Our model assumes that the densified regime initiates in the center of the foam and symmetrically propagates toward the plates through the elastic buckling of one layer of foam (of roughly one cell thickness) at a time, as shown in Fig. 2(*a*). The foam in the elastic regime below the densified regime (Region 1) is stationary while the foam in the elastic regime above the densified regime (Region 3) is moving downward with the upper plate at velocity $|\dot{h}|$, as shown in Fig. 2(*a*). Therefore, the densified regime (Region 2) is moving downward at velocity $\frac{1}{2}|\dot{h}|$. In the reference frame of the densified regime of the foam, the problem can be viewed as a completely symmetric problem with the elastic regimes (Regions 1 and 3) of the foam moving toward the densified regime, in opposite directions, at a speed of $\frac{1}{2}|\dot{h}|$. Since there is no flow across the center of the densified regime by symmetry, we analyze only the top half of the foam in the reference frame of the densified regime, as shown in Fig. 2(*b*). The problem is analyzed as two one-regime models with local reference heights $\frac{1}{2}h_e$ and $\frac{1}{2}h_d$ for the elastic and densified regimes, respectively, given as (Fig. 2)

$$h_e = \chi_{\text{el}}^* h \tag{16}$$

$$h_d = \chi_d h \tag{17}$$

The boundary conditions at the foam-plate interfaces are no flux conditions since the relative velocity of the fluid with respect to the foam is zero. Therefore, according to Darcy's law, the corresponding pressure gradients in the z-direction are zero at both foam-plate interfaces. Boundary conditions applied at the interface between the two regimes are given. The pressure field is taken to be continuous between the two regimes with a discontinuity in the pressure gradient, corresponding to the change in the permeability. In addition, a mass flux corresponding to the fluid exiting the layer undergoing elastic buckling enters both the linear-elastic and the densified regimes at the interface between the two regimes. Since the surface area between the layer undergoing elastic buckling and the linear-elastic and densified regimes is much greater than the surface area of the buckling layer at the free surface of the foam, we assume all of the fluid exiting the layer undergoing elastic buckling flows vertically into either the elastic or the densified regimes and neglect the radial flow in the buckling layer out of the foam. The boundary conditions for the two-regime problem are given as

$$P_d^* = P_e^* = 0 \quad \text{on} \quad r = R \tag{18a}$$

$$\frac{\partial P_d^*}{\partial z} = 0 \quad \text{on} \quad z = 0 \tag{18b}$$

$$\frac{\partial P_e^*}{\partial z} = 0 \quad \text{on} \quad z = \tfrac{1}{2}h \tag{18c}$$

$$\frac{\partial P_d^*}{\partial z} = \frac{-(1-\alpha)\mu \dot{h}}{2k_d} \quad \text{on} \quad z = \tfrac{1}{2}h_d \tag{18d}$$

$$\frac{\partial P_e^*}{\partial z} = \frac{\alpha \mu \dot{h}}{2k_{\text{el}}^*} \quad \text{on} \quad z = \tfrac{1}{2}h_d \tag{18e}$$

$$P_d^* = P_e^* \quad \text{on} \quad z = \tfrac{1}{2}h_d \tag{18f}$$

where α, determined below, is a constant representing the fraction of the flux into the linear-elastic regime, P_e^* is the pressure in the linear-elastic regime, and P_d^* is the pressure in the densified regime.

As before, Darcy's law is assumed to govern the flow of a viscous Newtonian fluid throughout each regime of the foam and is given as [14]

$$\nabla P^* = \frac{-\mu V}{k} \tag{19}$$

where V is the relative velocity of the fluid with respect to the foam, and k is the local permeability, which is assumed to be isotropic. Taking the gradient of both sides of Eq. (19), applying continuity for an incompressible Newtonian fluid, and considering there is no variation in the velocity of the foam within each region give Laplace's equation

$$\nabla^2 P^* = \frac{\partial^2 P^*}{\partial r^2} + \frac{1}{r}\frac{\partial P^*}{\partial r} + \frac{1}{r^2}\frac{\partial^2 P^*}{\partial \theta^2} + \frac{\partial^2 P^*}{\partial z^2} = \frac{-\mu \nabla \cdot V}{k} = 0 \tag{20}$$

A well known method of solving Laplace's equation in cylindrical coordinates is separation of variables. We assume the pressure is not a function of the circumferential direction (θ-direction) and propose a solution in the form

$$P^* = R(r)Z(z) \tag{21}$$

Substituting Eq. (21) into Eq. (20) and dividing through by $R(r)Z(z)$ give

$$\frac{1}{R(r)}\frac{\partial^2 R(r)}{\partial r^2} + \frac{1}{rR(r)}\frac{\partial R(r)}{\partial r} + \frac{1}{Z(z)}\frac{\partial^2 Z(z)}{\partial z^2} = 0 \tag{22}$$

Since the first two terms are functions of r only and the last term is a function of z only, Eq. (22) can be broken up into the following two equations:

$$\frac{1}{Z(z)}\frac{d^2 Z(z)}{dz^2} = -\eta \tag{23}$$

$$\frac{1}{R(r)}\frac{d^2R(r)}{dr^2}+\frac{1}{rR(r)}\frac{dR(r)}{dr}=\eta \tag{24}$$

where η is a constant. Equation (23) is a standard second order differential equation, which is readily solved. Equation (24) is one form of Bessel's equation and solutions can be expressed in terms of Bessel functions. Combining these solutions, the solution to Laplace's equation for the pressure distribution in either regime of the foam is given as

$$P_i^*=\sum_{n=1}^{\infty}(A_{ni}e^{k_nz}+B_{ni}e^{-k_nz})J_0(k_nr) \tag{25}$$

where the index i represents either the elastic regime or the densified regime with indices e and d, respectively, A_{ni}, B_{ni}, and k_n are constants, and J_0 is a zero order Bessel function of the first kind.

Applying both the Neumann and Dirichlet boundary conditions in Eqs. (18*a*)–(18*f*) to the solution to Laplace's equation given in Eq. (25), the pressure distribution throughout the foam can be determined. It is recognized that each term in Eq. (25) will satisfy the free surface boundary condition given by Eq. (18*a*) if

$$J_0(k_nR)=0 \tag{26}$$

Equation (26) therefore gives the values of k_n, corresponding to the zeros of the zero order Bessel function. The values can be determined from a table of Bessel functions. Typically, these solutions converge very quickly, so we assume that only the first five terms of the infinite series are necessary for most values of h/R. The corresponding values of k_n are given as

$$k_1=\frac{2.405}{R},\quad k_2=\frac{5.520}{R},\quad k_3=\frac{8.645}{R},\quad k_4=\frac{11.792}{R},\quad k_5=\frac{14.931}{R} \tag{27}$$

To solve for the unknowns A_{ni} and B_{ni}, the following orthogonality principle of zero order Bessel functions is utilized:

$$\int_0^R rJ_0(k_nr)J_0(k_mr)dr=0\quad \text{for } n\neq m \tag{28}$$

where $J_0(k_nr)$ is orthogonal to $J_0(k_mr)$. Applying the boundary conditions given by Eqs. (18*b*)–(18*e*) to Eq. (25), multiplying each side by r times a zero order Bessel function, and integrating allow for each coefficients A_{ni} and B_{ni} to be determined by the following set of equations:

$$(A_{nd}k_n-B_{nd}k_n)\int_0^R rJ_0^2(k_nr)dr=0 \tag{29}$$

$$(A_{ne}k_ne^{(1/2)k_nh}-B_{ne}k_ne^{-(1/2)k_nh})\int_0^R rJ_0^2(k_nr)dr=0 \tag{30}$$

$$(A_{nd}k_ne^{(1/2)k_nh_d}-B_{nd}k_ne^{-(1/2)k_nh_d})\int_0^R rJ_0^2(k_nr)dr=\frac{-(1-\alpha)\mu\dot{h}}{2k_d}\int_0^R rJ_0(k_nr)dr \tag{31}$$

$$(A_{ne}k_ne^{(1/2)k_nh_d}-B_{ne}k_ne^{-(1/2)k_nh_d})\int_0^R rJ_0^2(k_nr)dr=\frac{\alpha\mu\dot{h}}{2k_{\mathrm{el}}^*}\int_0^R rJ_0(k_nr)dr \tag{32}$$

Solving Eqs. (29)–(32) gives the coefficients A_{ni} and B_{ni} as

$$A_{nd}=\frac{-(1-\alpha)\mu\dot{h}RJ_1(k_nR)}{2k_d(k_nR)^2\sinh\left(\frac{1}{2}k_nh_d\right)[J_0^2(k_nR)+J_1^2(k_nR)]} \tag{33}$$

$$A_{ne}=\frac{\alpha\mu\dot{h}RJ_1(k_nR)}{k_{\mathrm{el}}^*(k_nR)^2(1-e^{k_nh_e})[J_0^2(k_nR)+J_1^2(k_nR)]} \tag{34}$$

$$B_{nd}=\frac{-(1-\alpha)\mu\dot{h}RJ_1(k_nR)}{2k_d(k_nR)^2\sinh\left(\frac{1}{2}k_nh_d\right)[J_0^2(k_nR)+J_1^2(k_nR)]} \tag{35}$$

$$B_{ne}=\frac{\alpha\mu\dot{h}RJ_1(k_nR)e^{k_nh_e}}{k_{\mathrm{el}}^*(k_nR)^2(1-e^{k_nh_e})[J_0^2(k_nR)+J_1^2(k_nR)]} \tag{36}$$

where $J_1(k_nR)$ is a first order Bessel function. Substituting Eqs. (33)–(36) into Eq. (25) and applying Eq. (26) give the adjusted pressure distribution in both the densified regime and the elastic regime as

$$P_d^*=\sum_{n=1}^{\infty}\frac{-(1-\alpha)\mu\dot{h}R\cosh(k_nz)J_0(k_nr)}{k_d(k_nR)^2\sinh\left(\frac{1}{2}k_nh_d\right)J_1(k_nR)},\qquad \varepsilon_{\mathrm{el}}^*\leq\varepsilon\leq\varepsilon_d,\quad 0\leq z\leq\tfrac{1}{2}h_d \tag{37}$$

$$P_e^*=\sum_{n=1}^{\infty}\frac{\alpha\mu\dot{h}R(e^{k_n(z-(1/2)h_d)}+e^{k_n(h_e-z+(1/2)h_d)})J_0(k_nr)}{k_{\mathrm{el}}^*(k_nR)^2(1-e^{k_nh_e})J_1(k_nR)},\qquad \varepsilon_{\mathrm{el}}^*\leq\varepsilon\leq\varepsilon_d,\quad \tfrac{1}{2}h_d\leq z\leq\tfrac{1}{2}h \tag{38}$$

Applying the remaining boundary condition in Eq. (18*f*), the constant α can be determined numerically. Since the terms of the pressure distribution given in Eqs. (37) and Eq. (38) decay rapidly, a good approximation to α can be given using only the first term in the series

$$\alpha=\frac{k_{\mathrm{el}}^*\tanh\left(\frac{1}{2}k_1h_e\right)}{k_{\mathrm{el}}^*\tanh\left(\frac{1}{2}k_1h_e\right)+k_d\tanh\left(\frac{1}{2}k_1h_d\right)} \tag{39}$$

The fraction of the flux into the linear-elastic regime α, as a function of strain, is given in Fig. 3. A force balance can be used to find an equivalent uniform stress distribution σ_f, applied to the top compression plate by integrating the pressure field in the elastic regime at $z=\frac{1}{2}h$ over the radius as follows:

$$\sigma_f\pi R^2=\int_0^R P_e^*|_{h/2}2\pi r dr,\qquad \varepsilon_{\mathrm{el}}^*\leq\varepsilon\leq\varepsilon_d \tag{40a}$$

$$\sigma_f\pi R^2=\left(\sum_{n=1}^{\infty}\frac{2\pi\alpha\mu\dot{h}R(2e^{k_n((1/2)h_e)})}{k_{\mathrm{el}}^*(k_nR)^2(1-e^{k_nh_e})J_1(k_nR)}\right)\left(\int_0^R rJ_0(k_nr)dr\right),\qquad \varepsilon_{\mathrm{el}}^*\leq\varepsilon\leq\varepsilon_d \tag{40b}$$

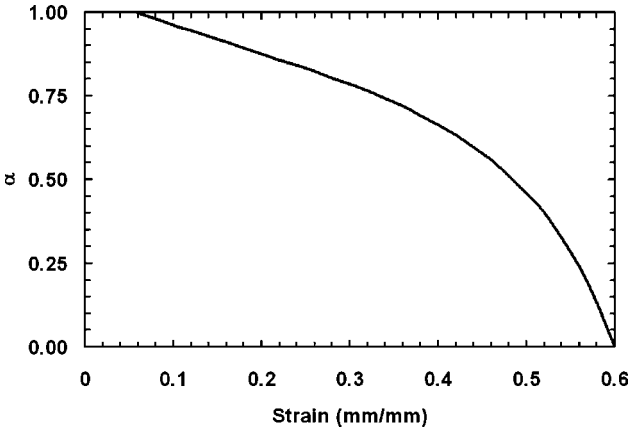

Fig. 3 The fraction of the flux into the linear-elastic regime (α) as a function of strain in the bimodal model

$$\sigma_f R^2 = \sum_{n=1}^{\infty} \left(\frac{4\alpha\mu\dot{h}R}{k_{\mathrm{el}}^{*}(k_n R)^2 (e^{-k_n((1/2)h_e)} - e^{k_n((1/2)h_e)}) J_1(k_n R)} \right) \times \left(\frac{R^2 J_1(k_n R)}{(k_n R)} \right), \quad \varepsilon_{\mathrm{el}}^{*} \leqslant \varepsilon \leqslant \varepsilon_d \tag{40c}$$

$$\sigma_f = \frac{-2\alpha\mu\dot{h}R}{k_{\mathrm{el}}^{*}} \sum_{n=1}^{\infty} \frac{1}{(k_n R)^3 \sinh\left(\frac{1}{2}k_n h_e\right)}, \quad \varepsilon_{\mathrm{el}}^{*} \leqslant \varepsilon \leqslant \varepsilon_d \tag{40d}$$

Equation (40*d*) is taken to be the contribution of the fluid to the stress-strain response of foam filled with a Newtonian fluid under dynamic compression in the two-regime model. The dependence of the response given by Eq. (40*d*) on strain is built in through the terms α and h_e, which are functions of the volume fraction of the cells remaining in the linear-elastic and densified regimes, and therefore, are functions of the strain.

3.4 Effect of Tortuous and Anisotropic Foam Microstructure. A discrepancy is typically found between analytical models for flow through porous media and experimental measurements. Models are often adjusted by an empirical constant, which accounts for the tortuous shape of the foam microstructure [15]. Similarly, empirical constants are also used to account for the tortuous microstructure of foam in studies of heat transfer through porous media. Glicksman [16] determined an efficiency factor of 2/3 accounted for the effective loss in the thermal conductivity of porous media. Furthermore, it is known that the permeability of low-density, open-cell foam is slightly anisotropic, which may also lead to deviations of the model presented in this analysis from experimental data. The combination of these effects necessitates the addition of empirical constant C to the model. Therefore, we propose that the stress contribution of a Newtonian fluid to the response of a fluid-filled foam under dynamic loading is given by

$$\sigma_f = \frac{-C\mu\dot{h}R^2}{8\Phi h k_e}, \quad 0 \leqslant \varepsilon \leqslant \varepsilon_{\mathrm{el}}^{*} \tag{41}$$

$$\sigma_f = \frac{-2C\alpha\mu\dot{h}R}{k_{\mathrm{el}}^{*}} \sum_{n=1}^{\infty} \frac{1}{(k_n R)^3 \sinh\left(\frac{1}{2}k_n h_e\right)}, \quad \varepsilon_{\mathrm{el}}^{*} \leqslant \varepsilon \leqslant \varepsilon_d \tag{42}$$

where C is a single constant to be determined by regression from experiments.

3.5 Squeezing Flow Between Parallel Plates. We now proceed to develop a more tractable model for the dynamic response of fluid-filled foam, which can be used to approximate the boundary value model in the lubrication limit where the aspect ratio of the foam is much greater than unity. We first consider a model for squeezing flow between two parallel plates in the absence of an open-cell foam where the lower plate is fixed and the upper plate is moving similar to Fig. 1. The flow is assumed to be incompressible and locally fully developed with no variation in the circumferential direction (θ-direction). The gravitational effects are assumed to be negligible. Since the flow is assumed to be dominated by viscous forces, inertial effects can also be neglected. The following velocity profiles are assumed:

$$V_r = V_r(r,z), \quad V_z = V_z(z), \quad V_\theta = 0 \tag{43}$$

where V_r, V_z, and V_θ are the velocity components in the radial (r), axial (z), and circumferential (θ) directions, respectively. Coupling the equation of continuity with the full Navier–Stokes equations of motion, this problem is readily solved. The equation of continuity and the Navier–Stokes equations of motion in the radial and axial directions reduce to

$$\frac{1}{r}\frac{\partial(rV_r)}{\partial r} + \frac{\partial V_z}{\partial z} = 0 \tag{44}$$

$$\mu\left(\frac{\partial}{\partial r}\frac{1}{r}\frac{\partial}{\partial r}(rV_r) + \frac{\partial^2 V_r}{\partial z^2}\right) - \frac{\partial P}{\partial r} = 0 \quad (r\text{-direction}) \tag{45}$$

$$\mu\left(\frac{1}{r}\frac{\partial}{\partial r}r\frac{\partial V_z}{\partial r} + \frac{\partial^2 V_z}{\partial z^2}\right) - \frac{\partial P}{\partial z} = 0 \quad (z\text{-direction}) \tag{46}$$

where P is the local pressure within the fluid. To solve Eqs. (44)–(46), we initially impose a lubrication approximation in which the square of the ratio of the characteristic dimension in the radial flow direction (R) to that in the axial compression direction (h) is assumed to be much greater than unity, $(R/h)^2 \gg 1$. The resulting equations of motion are given as

$$\mu\left(\frac{\partial^2 V_r}{\partial z^2}\right) - \frac{\partial P}{\partial r} = 0 \quad (r\text{-direction}) \tag{47}$$

$$\frac{\partial P}{\partial z} = 0 \quad (z\text{-direction}) \tag{48}$$

The corresponding boundary conditions are

$$V_r|_{z=h} = 0, \quad \left.\frac{\partial V_r}{\partial z}\right|_{z=h/2} = 0, \quad V_z|_{z=0} = 0, \quad V_z|_{z=h} = \dot{h}, \tag{49}$$

$$P|_{r=R} = P_a$$

where R is the radius of the plates, h is given as the current distance between the bottom plate and the top plate, P_a is the atmospheric pressure on the free surface, and the magnitude of the velocity of the top plate is given by $|\dot{h}|$, where $\dot{h}$ is the time rate of change of the distance between the two plates. Solving Eqs. (47) and (48) gives the pressure profile as

$$P - P_a = \frac{3\mu\dot{h}}{h^3}(r^2 - R^2) \tag{50}$$

The pressure distribution is found to be independent of the z- and θ-directions. We propose that the pressure field given by Eq. (50) for squeezing, viscous flow is similar to the pressure field for squeezing flow in a low-density foam. Therefore, in the lubrication limit, the pressure field for an incompressible, viscous Newtonian flow through a low-density foam is assumed to be independent of the z- and θ-directions.

3.6 Stress-Strain Response in the Lubrication Limit. The model of viscous squeezing flow between two parallel plates de-

scribed above does not accurately describe the flow field for axial compression of a low-density, reticulated foam filled with a Newtonian fluid because of the nonlinear behavior of the foam under deformation; however, we assume that the pressure field of the parallel plate model is representative of that found in a lubrication model of a fluid-filled foam, such that the pressure field is independent of the z- and θ-directions.

Using this assumption, we extend the model presented by Dawson et al. [7] for reticulated foam under compressive strain. We consider the case of axial compression of a cylindrical foam specimen where the characteristic radius is much greater than the characteristic height. The initial radius and height of the specimen are taken to be R and h_0. As the foam undergoes compression, the radius of the specimen remains unchanged while the instantaneous height is given as $h(t)$. Compression occurs between two plates where the lower plate is assumed to be fixed and the magnitude of the velocity of the upper plate is $|\dot{h}|$, where $\dot{h}$ is the time rate of change of the height of the foam, as shown in Figs. 1 and 2. This analysis considers both the response at strains less than the elastic buckling strain and the response at strains greater than the elastic buckling strain but less than the densified strain. We first consider the single regime problem with strain less than the elastic buckling strain. Following the same methodology as used in Eqs. (12)–(14), the average radial velocity of the fluid, V_e, and the local pressure, P, in the elastic regime can be determined. As before, neglecting inertial effects, a force balance can be used to find an equivalent uniform stress distribution σ_f, applied to the top compression plate by integrating the pressure field given in Eq. (14) over the radius giving

$$\sigma_f = \frac{-\mu \dot{h} R^2}{8\Phi h k_e}, \quad 0 \le \varepsilon \le \varepsilon^*_{\mathrm{el}} \tag{51}$$

For strains beyond the elastic buckling strain but less than the densified strain, the model is taken to be a two-regime model, as shown in Fig. 2. Based on the previous assumptions regarding no axial variations in the pressure field, the pressure drop from the any radius r to the outer radius R is assumed to be the same in both the elastic region and the densified region. Coupling this relation between the pressure drops in each region with Eq. (13) gives

$$\frac{V_e}{k^*_{\mathrm{el}}} = \frac{V_d}{k_d}, \quad \varepsilon^*_{\mathrm{el}} \le \varepsilon \le \varepsilon_d \tag{52}$$

where V_d is the velocity of the fluid at any radius r in the densified region. Using Eq. (52), mass conservation about a cylindrical volume at any given r gives

$$V_e = \frac{-\dot{h} k^*_{\mathrm{el}} r}{2h\Phi(\chi^*_{\mathrm{el}} k^*_{\mathrm{el}} + \chi_d k_d)}, \quad \varepsilon^*_{\mathrm{el}} \le \varepsilon \le \varepsilon_d \tag{53}$$

Coupling Darcy's law with Eq. (53) gives the pressure gradient across the specimen $\partial P/\partial r$ for viscous Newtonian flow [14] as follows:

$$\frac{\partial P}{\partial r} = \frac{\mu \dot{h} r}{2h\Phi(\chi^*_{\mathrm{el}} k^*_{\mathrm{el}} + \chi_d k_d)}, \quad \varepsilon^*_{\mathrm{el}} \le \varepsilon \le \varepsilon_d \tag{54}$$

Integrating Eq. (54) and applying the atmospheric pressure boundary condition at the free surface give

$$P - P_a = \frac{\mu \dot{h}}{4h\Phi(\chi^*_{\mathrm{el}} k^*_{\mathrm{el}} + \chi_d k_d)}(r^2 - R^2), \quad \varepsilon^*_{\mathrm{el}} \le \varepsilon \le \varepsilon_d \tag{55}$$

As before, neglecting inertial effects, a force balance can be used to find an equivalent uniform stress distribution σ_f, applied to the top compression plate by integrating the pressure field over the radius giving

Table 1 Table of coefficients for the bimodal model as a function of the aspect ratio of the foam and for the lubrication model, corresponding to Eqs. (57) and (58).

R/h	C_1 (ε=0.05)	C_1 (ε=0.30)	C_1 (ε=0.60)
$\frac{1}{2}$	0.031	0.111	0.827
1	0.057	0.127	0.501
2	0.069	0.132	0.404
4	0.072	0.133	0.378
8	0.073	0.133	0.371
16	0.074	0.133	0.369
32	0.074	0.133	0.368
Lubrication	0.076	0.137	0.380

$$\sigma_f \pi R^2 = \int_0^R (P - P_a)|_h 2\pi r dr, \quad \varepsilon^*_{\mathrm{el}} \le \varepsilon \le \varepsilon_d \tag{56a}$$

$$\sigma_f = \frac{-\mu \dot{h} R^2}{8h\Phi(\chi^*_{\mathrm{el}} k^*_{\mathrm{el}} + \chi_d k_d)}, \quad \varepsilon^*_{\mathrm{el}} \le \varepsilon \le \varepsilon_d \tag{56b}$$

3.7 Convergence of the Boundary Value Model to the Lubrication Model. In this analysis, we consider the convergence of the boundary value model to the lubrication model in the limit of large R/h. A parametric study is used to compare the model given by Eqs. (41) and (42) for varying ratios of R/h to the lubrication model given by Eqs. (51), (56*a*), and (56*b*). The models can be readily compared if each model is rewritten in the following form:

$$\sigma_f = -C_1\left(\frac{\mu \dot{h} R^2}{h k_e}\right), \quad 0 \le \varepsilon \le \varepsilon^*_{\mathrm{el}} \tag{57}$$

$$\sigma_f = -C_1\left(\frac{\mu \dot{h} R^2}{h k^*_{\mathrm{el}}}\right), \quad \varepsilon^*_{\mathrm{el}} \le \varepsilon \le \varepsilon_d \tag{58}$$

where C_1 is the dimensionless coefficient corresponding to the numerically evaluated portion of each model, including the empirically derived coefficient C, which will be determined in Sec. 4. For strains less than the elastic buckling strain, the coefficient C_1 for the model presented in this paper is independent of the aspect ratio of the specimen. Therefore, for strains less than the elastic buckling strain, the model presented in this analysis is identical to that presented in the lubrication analysis for all aspect ratios of the foam, so there is no difference in the coefficients C_1, for the lubrication and boundary value models in this regime. However, for strains less than the densified strain but greater than the elastic buckling strain, the coefficient C_1 for the model presented in this paper is a function of the aspect ratio of the foam and the strain while that for the lubrication model is only a function of strain. Therefore, the convergence of this bimodal model toward the lubrication model with increasing aspect ratio is presented for three different strains in Table 1. To determine the coefficient C_1 for both the bimodal model presented in this analysis and the lubrication model, the necessary parameters are numerically evaluated based on the data presented in this analysis. The permeability of the foam at the densified strain is taken to be 20% of that of the foam at the elastic buckling strain, $k_d = 0.20 k^*_{\mathrm{el}}$, the elastic buckling strain is taken to be $\varepsilon^*_{\mathrm{el}} = 0.05$, the densified strain is taken to be $\varepsilon_d = 0.60$, and the porosity is taken to be $\Phi = 0.97$ (after Dawson et al. [7]).

4 Experiments

4.1 Materials. Specimens of open-cell, flexible, polyester-based polyurethane foams (New Dimension Industries, Moonachie, NJ), with nominal cell diameters of 175 μm, 210 μm, and

235 μm based on manufacturers' specifications (corresponding to grades of 90 ppi, 80 ppi, and 70 ppi, respectively, were used in the tests. The densities of the foams ranged from 0.0318 g/cm^3 to 0.0322 g/cm^3. Based on the manufacturer's value of the density of the solid polyurethane (ρ_s=1.078 g/cm^3) the relative density of the foams was taken to be $\rho_0^*/\rho_s \cong 0.03$. Using Eq. (4), the corresponding fully densified strain is determined to be ε_D=0.958. The foam was cut into uniform cylindrical specimens with diameter and height, D=25.4 mm and h=12.8 mm, respectively. The dimensions of each sample were measured using a digital caliper accurate to within 0.01 mm. The Newtonian fluid used in these experiments is glycerol where the density and viscosity are measured to be ρ=1260 kg/m^3 and μ=1.1 Pa/s at 23°C.

4.2 Experimental Procedure. Prior to testing, each sample was saturated with glycerol. Since the viscosity of glycerol is a strong function of temperature, it was heated to 40°C before saturation to aid in the saturation process. Samples were compressed by machine, submerged in glycerol, and uncompressed at 1 mm/s. Hager and Craig [17] demonstrated that the indentation force deflection loss (a measure of the load bearing capability of flexible polyurethane foam) of polyurethane foam compressed to 0.75 strain for a short duration of time is almost completely recoverable. Therefore, a compressive strain of 0.75 was selected for saturating the sample to minimize the microstructural damage caused by the filling process. After saturation, the fluid-filled foam was brought to a steady temperature of 23°C and allowed to recover. Based on the data for the recovery of low-density polyurethane foam after 0.75 compression presented by Hager and Craig [17], a recovery time of 2 h was selected.

The compressive stress-strain response of each glycerol-filled specimen was measured with the rise direction of the foam parallel to the direction of loading, from 0 to 0.60 strain over a range of strain rates from $\dot{\varepsilon}=2.5\times10^{-3}$ s^{-1} to 10^1 s^{-1}. For strain rates of $\dot{\varepsilon}=1$ s^{-1} or less, a texture analyzer (TA XT Plus, Stable Microsystems, Hamilton, MA) was used at a constant strain rate; for strain rates greater than $\dot{\varepsilon}=1$ s^{-1}, an Instron testing machine (Instron Model 1321, Instron Corp., Canton, MA) was used at constant velocity. During testing, the temperature was maintained at 23.0±0.1°C to ensure that the glycerol retains a constant viscosity. Since the flow is assumed to be instantaneously fully developed, the model presented in this paper is applicable to both constant velocity and constant strain rate loading.

4.3 Experimental Results. A typical plot of the stress-strain response of the 90 ppi foam filled with glycerol loaded at a constant strain rate of $\dot{\varepsilon}=0.01$ s^{-1} is shown in Fig. 4. This strain rate is assumed to most accurately represent quasistatic loading where the loading is slow enough that the fluid is not expected to significantly contribute to the response of the specimen yet fast enough that viscoelastic effects in the foam are negligible. Using Fig. 4, the parameters and constants governing the response of the foam structure, given by Eqs. (1)–(5), can be determined. A detailed discussion of the microstructural behavior of open-cell foam under compressive loading in the direction of the rise direction of the foam is given by Gong and Kyriakides [18]. They discussed the complex local and global buckling behavior of low-density, open-cell foam. We consider a simplified model for the elastic buckling strain $\varepsilon_{\mathrm{el}}^*$, taken to be the average value of the strain at which the behavior of the foam begins to deviate from the linear-elastic regime and the strain corresponding to the peak stress prior to the plateau region, as shown in Fig. 4. The elastic buckling stress σ_{el}^* is taken to be the stress at the elastic buckling strain $\varepsilon_{\mathrm{el}}^*$. As previously discussed, ε_p^* corresponds to the strain at which the stress at the end of the plateau region is equal to the elastic buckling stress, as shown in Fig. 4. The values for the elastic buckling strain $\varepsilon_{\mathrm{el}}^*$, the strain at which the stress at the end of the plateau stress is equal to the elastic buckling stress, and the corresponding

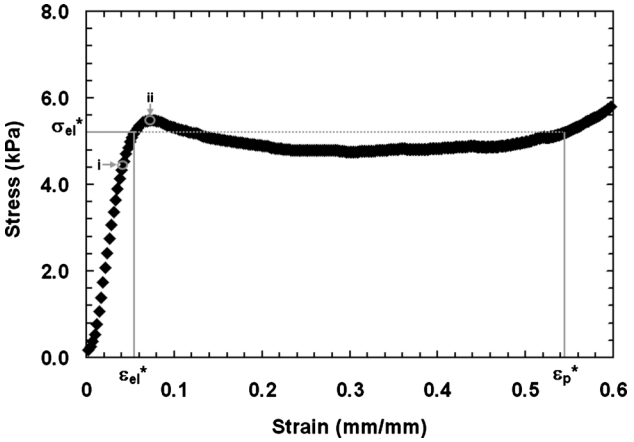

Fig. 4 Stress-strain response of the 90 ppi foam under a quasistatic load rate of $\dot{\varepsilon}=1\times10^{-2}$ s^{-1}. (i) Strain corresponding to deviation from linear-elastic regime. (ii) Strain corresponding to peak stress before the plateau region.

constant are provided for grades of 70 ppi, 80 ppi, and 90 ppi foams in Table 2. The final unknown parameter in the model for the response of the foam structure given by Eqs. (1)–(5) is the effective modulus. The effective modulus of the foam is found to depend strongly on the strain rate due to viscoelastic effects in the quasistatic loading regime and microinertial effects and localization phenomenon in the high rate loading regime. The effective modulus used in Eq. (1) for each grade of foam is found to be well approximated by $E^*=X\ln(\dot{\varepsilon}/\dot{\varepsilon}_0)+Y$ over the strain rates presented in this analysis where $\dot{\varepsilon}$ is taken to be $\dot{\varepsilon}=1$ s^{-1} and the constants X and Y are provided in Table 2. The elastic buckling strains correspond well with previous literature on low-density foams [8]. To plot the fluid model, the permeabilities at the elastic buckling strain and at the densified strain are required. These values are obtained using the equations for the local permeability and the corresponding intrinsic permeability at zero strain k_0. It has been observed that large strain compression causes microstructural damage to low-density foam, altering the permeability at zero strain [19]. Therefore, the permeability at zero strain for each specimen was measured after the specimens were subjected to the compressive filling technique used for saturating the foam with glycerol. The permeability was measured using the technique given by Dawson et al. [7]. Table 3 provides the measured permeability at zero strain and the corresponding permeabilities utilized in modeling the stress-strain response.

A typical plot of the stress-strain response for the 70 ppi foam filled with glycerol loaded at a constant strain rate of $\dot{\varepsilon}=1.0$ s^{-1} is given in Fig. 5. The actual response of the fluid-filled foam is plotted along with the model for the total contribution to the stress-strain response, which results from the combination of the solid contribution given by Eqs. (1)–(3) and the fluid contribution given by Eqs. (41) and (42). The solid and fluid contributions are also given separately to demonstrate their relative contributions.

To fit the constant C given in Eqs. (41) and (42), a measure of

Table 2 Static parameters and constants. The elastic buckling strain $\varepsilon_{\mathrm{el}}^*$, the strain at which the stress begins to exceed the plateau stress ε_p^*, and the constants *X*, *Y*, and *D* (Eq. (5))

Foam grade (ppi)	$\varepsilon_{\mathrm{el}}^*$	ε_p^*	*X* (Pa)	*Y* (Pa)	*D*
70	0.058	0.55	1.07*E*+04	1.35*E*+05	2.3
80	0.049	0.54	1.28*E*+04	1.70*E*+05	2.3
90	0.057	0.55	1.09*E*+04	1.42*E*+05	2.3

Table 3 Permeability data for precompressed foam. The permeability at zero strain k_0, for each grade of foam, is given after being subjected to the saturation process. The permeabilities at the elastic buckling strain and densified strain are determined using the equations supplied in Eqs. (8)–(10)

Foam grade (ppi)	k_0 $(1\times10^{-9}\ \mathrm{m}^2)$	k^*_{el} $(1\times10^{-9}\ \mathrm{m}^2)$	k_d $(1\times10^{-9}\ \mathrm{m}^2)$
70	5.82	5.45	1.28
80	5.21	4.93	1.04
90	4.68	4.39	0.85

the goodness of fit is established. The measure for the goodness of fit R^2 is taken to be the sum of the squares of the difference between the experimental values and the average experimental value divided by the sum of the squares of the difference between the experimental values and the predicted values. This measure of the goodness of fit was maximized, over the sample of experimental data discussed in the following sections, to establish the empirical constant.

In Fig. 6, we show the stress response of the 70 ppi foam filled with glycerol at $\varepsilon=0.60$ strain, corresponding to an aspect ratio of 2.5, plotted against the strain rate. Each data point is the average of three experiments with error bars corresponding to 1 standard deviation. The error bars for most data points are not apparent since they are smaller than the size of the data points. The fluid and solid contributions of the stress, given by Eqs. (2), (3), and (42), respectively, are plotted separately showing their relative contributions. In Fig. 7, we show the stress at $\varepsilon=0.30$ strain and $\varepsilon=0.60$ strain, corresponding to aspect ratios of 1.4 and 2.5, respectively, for all three grades of reticulated foam filled with glycerol plotted against the strain rate. Each data point is again the average of three experiments with error bars corresponding to 1 standard deviation. The total contribution to the stress-strain response, which results from the combination of the solid contribution given by Eqs. (2) and (3) and the fluid contribution given by Eq. (42), is also shown in Fig. 7.

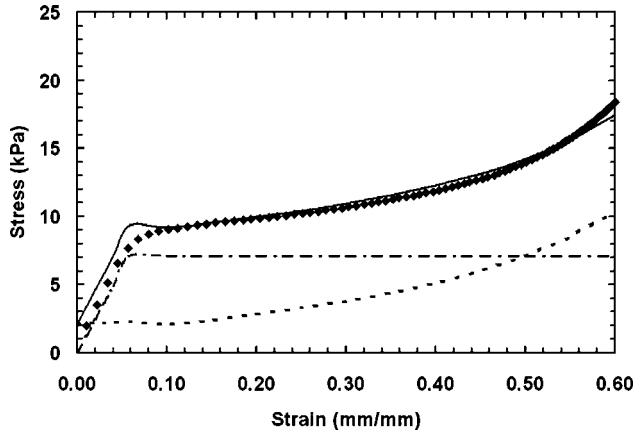

Fig. 5 Stress plotted against strain for 70 ppi foam. Experimental data (♦). Contribution to the stress response of fluid model given by Eqs. (41) and (42) (---), the solid model given by Eqs. (1) and (3) (–·–), and the total model (—).

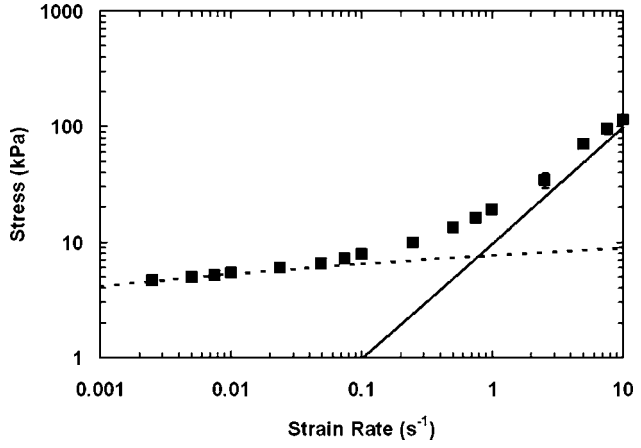

Fig. 6 Stress plotted against strain rate for 70 ppi foam at $\varepsilon=0.60$. Experimental data (■), the contribution to the stress response of fluid model given by Eqs. (41) and (42) (—) and solid model given by Eqs. (1) and (3) (---).

All of the data used to generate the plots in Fig. 7 are used to determine the empirical constant C. Using each data point along the 0.3 and 0.6 strain curves, which consist of the average of three experimental points, for all three foam grades, the empirical constant is determined to be $C=0.59$. Based on the data in Fig. 7, the R^2 values for each grade of foam at both $\varepsilon=0.30$ and $\varepsilon=0.60$ are given in Table 4; it is clear that the model describes the data well up to the densified strain for a range of foam grades and strain rates, as shown in Fig. 7. The empirical constant C, which primarily accounts for the tortuous and anisotropic microstructure of the foam, is independent of all of the parameters considered in this analysis. Figure 7 supports this initial assumption, demonstrating that C is independent of the cell size of low-density foam, the aspect ratio of the foam, the strain imposed on the foam, and the strain rate applied to the foam. Additional experimental studies, not presented here, that vary the aspect ratio of the foam also support this proposal. Using $C=0.59$, the model given by Eq. (42) accurately describes the data for fluid-filled foam samples over several orders of magnitude of strain rate with an aspect ratio of approximately 10 at $\varepsilon=0.60$.

5 Discussion

A boundary value model for the contribution of viscous Newtonian fluid flow to the stress-strain response of a fluid-filled foam under dynamic compression is given by Eqs. (41) and (42). The model governing viscous flow in the bimodal regime of the foam is given in the form of an infinite series of Bessel functions. As expected, this solution converges rapidly with an increasing number of terms, such that the boundary value model is readily evaluated numerically with only the first few terms. Based on the permeability studies of Dawson et al. [7], the models presented in this analysis are taken to be applicable for all grades of low-density foam and independent of whether the orientation of the rise direction of the foam is perpendicular or parallel to the direction of fluid flow. As previously discussed, the models in this analysis assume that the flow is dominated by viscous forces, which is shown to be the case for nearly all achievable strain rates. The boundary value model further assumes an instantaneous change in the velocity field of the foam at the elastic buckling strain ε^*_{el}, which is the strain at which the model transitions from the single regime to the bimodal regime. The transition behavior between these two regimes is neglected, which results in a small discontinuity in the stress response of the boundary value model. However, as the aspect ratio of the foam R/h is increased, the effect of the assumed velocity field of the foam becomes negligible, and the boundary value model rapidly approaches a continuous solution. In addition, with increasing R/h, the bimodal model becomes independent of the location of the densified bands of the foam.

The boundary value model presented in this analysis is found to describe the experimental results presented in this paper for foam grades varying from 70 ppi to 90 ppi and strain rates varying from $\dot{\varepsilon}=2.5\times10^{-3}\ \mathrm{s}^{-1}$ to $10^{1}\ \mathrm{s}^{-1}$ well. All of the strain rates in these experiments satisfy the viscous flow requirements of the

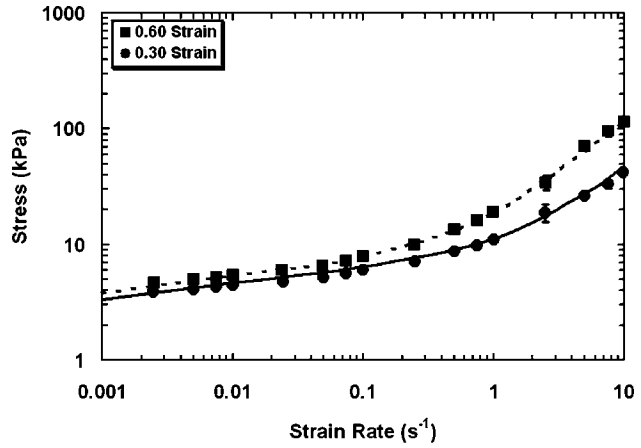

(*a*)

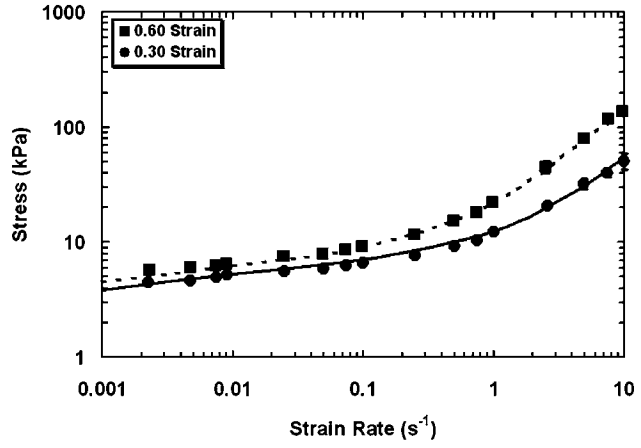

(*b*)

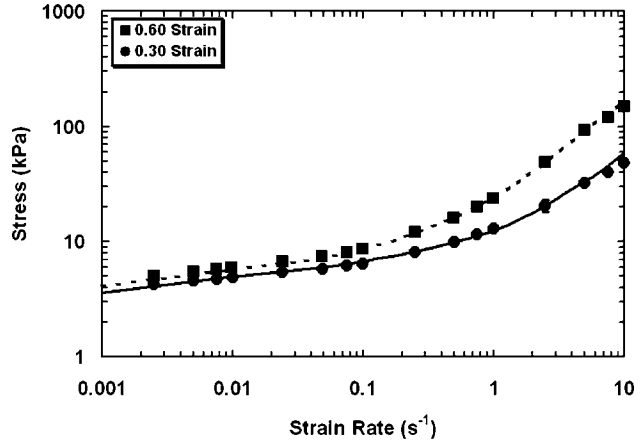

(*c*)

Fig. 7 (*a*) Stress plotted against strain rate for 70 ppi foam. Experimental data at 0.60 strain (■), and 0.30 strain (●), respectively. Model given by combining Eqs. (2) and (3) with Eq. (42) at $\varepsilon=0.30$ (—) and $\varepsilon=0.60$ (---). (*b*) Stress plotted against strain rate for 80 ppi foam. Experimental data at 0.60 strain (■), and 0.30 strain (●), respectively. Model given by combining Eqs. (2) and (3) with Eq. (42) at $\varepsilon=0.30$ (—) and $\varepsilon=0.60$ (---). (*c*) Stress plotted against strain rate for 90 ppi foam. Experimental data at 0.60 strain (■), and 0.30 strain (●), respectively. Model given by combining Eqs. (2) and (3) with Eq. (42) at $\varepsilon=0.30$ (—) and $\varepsilon=0.60$ (---).

Table 4 The measure for the goodness of fit of the boundary value model at 0.30 and 0.60 strains for each grade of foam

Foam grade (ppi)	R^2	
	0.30 strain	0.60 strain
70	0.97	0.99
80	0.99	0.99
90	0.95	0.99

models with $\mathrm{Re}<1$. The maximum Reynolds number in the experiments was found to be $\mathrm{Re}=0.017$, which corresponds to strain rate of $\dot{\varepsilon}=10\ \mathrm{s}^{-1}$ in a 70 ppi foam with an average cell diameter of 235 μm.

Figure 5 shows the individual contributions of both the solid model and the boundary value fluid model to the model of the total stress-strain response of the 70 ppi fluid-filled foam. The total model fits the data well over the entire range of interest, slightly overestimating the response at low strains. The previously discussed discontinuity in the models near the buckling strain is evident but shown to be negligible. Furthermore, Figs. 6 and 7 demonstrate that the boundary value model is representative of the actual response of the fluid-filled foam at both $\varepsilon=0.30$ and $\varepsilon=0.60$ for a range of foam grades and strain rates. The standard deviations of nearly all of the data are observed to be very small, on the order of the size of the data point. Overall, the goodness of fit measure given in Table 4 demonstrates that the boundary value model fits the data well for all grades of foam at both $\varepsilon=0.30$ and $\varepsilon=0.60$ for the range of strain rates considered. The boundary value model also fits the data well over all strains less than the densified strain, but the strains of $\varepsilon=0.30$ and $\varepsilon=0.60$ were selected as representative strains. The empirical constant $C=0.59$ primarily accounts for the tortuous and anisotropic microstructure of the foam and is found to be similar to the efficiency factor of $2/3$ found by Glicksman [16] in his study of the thermal conductivity of porous media. Furthermore, the empirical constant is proposed to be independent of all of the parameters considered in this analysis. Figure 7 supports this proposal demonstrating that C is independent of the cell size of low-density foam, the aspect ratio of the foam, the strain of the foam, and the strain rate of the foam.

While the boundary value model is readily evaluated and compared with experimental results, extending it to a more advanced study of dynamic loading of non-Newtonian fluid-filled foam is challenging. However, this model is useful in validating the applicability of the more tractable lubrication model, which assumes the radius of the foam is much greater than the height of the foam. The boundary value model is found to converge rapidly to within 5% of the lubrication model for aspect ratios greater than 4 ($R/h>4$). The small discrepancy between the coefficient for the lubrication model and that for the boundary value model may be attributed to the fact that the lubrication model assumes a uniform radial flow, neglects pressure gradients in the z-direction, and neglects the flow in the z-direction; whereas the boundary value model does not make these assumptions.

Table 1 demonstrates that as R/h is increased, the numerical coefficients at $\varepsilon=0.05$ and $\varepsilon=0.30$ strain increase asymptotically while the coefficient at $\varepsilon=0.60$ strain decreases asymptotically. At any given strain, the coefficient C_1 is governed primarily by the following two factors: the aspect ratio of the foam sample and the distance between the collapsing band and the compression plate. For all strains as R/h is decreased, the dependence of the stress, given by Eq. (58), on R/h also decreases. In the limit of very small R/h, the stress contribution of the fluid becomes completely independent of R/h.

At $\varepsilon=0.60$ strain, the stress is independent of the distance between the collapsing band and the compression plate $(1/2h_e)$ since the collapsing band is effectively always at the interface

between the compression plate and the foam. Therefore, it is expected that as R/h decreases, the coefficient C_1 would increase proportionally, such that the stress is independent of R/h in the limit of very small R/h. However, at 0.05 and 0.30 strains, the distance between the collapsing band and the compression plate $(1/2h_e)$ is also an important factor, which strongly influences the coefficient C_1. As R/h is decreased, the relative distance between the fluid in the collapsing band and the compression plate $(1/2h_e)$ to that of the fluid in the collapsing band and the free surface $(\sim R)$ increases; therefore, it is expected that the overall stress on the compression plate would decrease. For lower strains, this effect is more pronounced since the band is effectively farther from the compression plate, explaining the phenomenon observed in Table 1.

In the limit that $R/h \gg 1$, the effect of the distance between the collapsing bands and the compression plate is found to be inconsequential for all strains, and the stress becomes independent of the vertical location of the collapsing bands. Table 1 demonstrates that the model presented in this analysis becomes approximately independent of the aspect ratio of the foam for $R/h > 4$. As expected, this indicates that the lubrication model provides a good approximation to the flow for a large range of R/h values. Overall, the convergence of the more comprehensive boundary value model toward the lubrication model strongly supports the lubrication analysis. This is an important finding since the lubrication model is readily extended to more complex analyses, such as the study of the stress-strain response and energy absorption capabilities of a foam filled with a rate-dependent non-Newtonian fluid under dynamic loading.

6 Conclusion

In this paper, a comprehensive boundary value model for the contribution of viscous Newtonian fluid flow to the stress-strain response of a fluid-filled, elastomeric foam under dynamic compression is presented. Experimental results strongly support this model for a variety of foam grades over several orders of magnitude of strain rate. A simple explicit analytic solution based on a lubrication approximation is also presented. The robust boundary value model is found to converge rapidly toward the lubrication model as the aspect ratio of the foam is increased. This validation of the lubrication model is important since it is more readily extended to more complex analyses, such as the dynamic response of foam filled with a non-Newtonian fluid. Furthermore, using a lubrication model, both the Newtonian and non-Newtonian models can be extended to determine the energy absorption capabilities of a fluid-filled foam under dynamic loading, which is critical to the development of composite armor capable of absorbing energy and impeding shock waves.

Acknowledgment

This paper benefited from the insightful assistance provided by Professor Chiang Mei of the Department of Civil and Environmental Engineering, Massachusetts Institute of Technology. This research was performed while on appointment as a National Defense Science and Engineering Graduate Fellow administered by the American Society for Engineering Education (ASEE). This material is based upon work supported by the National Science Foundation under Grant No. 0408259.

Appendix

The velocity profiles in the absence of foam for the analysis in Sec. 3.5 are given as

$$V_r(r,z) = \frac{3\dot{H}r}{H}\left(\left(\frac{z}{H}\right)^2 - \frac{z}{H}\right) \tag{A1}$$

$$V_z(r,z) = 6\dot{H}\left(\frac{1}{2}\left(\frac{z}{H}\right)^2 - \frac{1}{3}\left(\frac{z}{H}\right)^3\right) \tag{A2}$$

References

[1] Cheeseman, B., and Bogetti, T., 2003, "Ballistic Impact Into Fabric and Compliant Composite Laminates," Compos. Struct., **61**, pp. 161–173.
[2] Bettin, G., and McKinley, G. H., 2005, "High Deformation Rate Behavior of Polymeric Foams Filled With Concentrated Silica Suspensions," The Society of Rheology 77th Annual Meeting.
[3] Hilyard, N. C., 1971, "Observations on the Impact Behaviour of Polyurethane Foams; II. The Effect of Fluid Flow," J. Cell. Plast., **7**, pp. 84–90.
[4] Rehkopf, J., Brodland, G., and McNeice, G., 1996, "Experimentally Separating Fluid and Matrix Contributions to Polymeric Foam Behavior," Exp. Mech., **36**, pp. 1–6.
[5] Mills, N., and Lyn, G., 2002, "Modeling Air Flow in Impacted Polyurethane Foam," Cell. Polym., **21**, pp. 343–365.
[6] Schraad, M., and Harlow, F., 2006, "A Multi-Field Approach to Modeling the Dynamic Response of Cellular Materials," Int. J. Mech. Sci., **48**, pp. 85–106.
[7] Dawson, M., Germaine, J., and Gibson, L., 2007, "Permeability of Open-Cell Foams Under Compressive Strain," Int. J. Solids Struct., **44**, pp. 5133–5145.
[8] Gibson, L. J., and Ashby, M. F., 1997, *Cellular Solids—Structures and Properties*, 2nd ed., Cambridge University Press, Cambridge.
[9] Brace, W., 1977, "Permeability From Resistivity and Pore Shape," J. Geophys. Res., **82**, pp. 3343–3349.
[10] Comiti, J., Sabiri, N., and Montillet, A., 2000, "Experimental Characterization of Flow Regimes in Various Porous Media—III: Limit of Darcy's or Creeping Flow Regime for Newtonian and Purely Viscous Non-Newtonian Fluids," Chem. Eng. Sci., **55**, pp. 3057–3061.
[11] Gent, A., and Rusch, K., 1966, "Permeability of Open-Cell Foamed Materials," J. Cell. Plast., **2**, pp. 46–51.
[12] Tek, M., 1957, "Development of a Generalized Darcy Equation," J. Pet. Technol., **9**(6), pp 45–47.
[13] Dybbs, A., and Edwards, R. V., 1984, "A New Look at Porous Media Fluid Mechanics—Darcy to Turbulent," *Fundamentals of Transport Phenomna in Porous Media*, J. Bear and Y. Corapcioglu, eds., Martinus Nishoff, Dordrecht, pp. 199–256.
[14] Darcy, H., 1856, *Les Fontaines Publiques de la Ville de Dijon*, Dalmont, Paris.
[15] Comiti, J., and Renaud, M., 1988, "A New Model for Determining Mean Structure Parameters of Fixed Beds From Pressure Drop Measurements: Applications to Beds Packed With Parallelpipedal Particles," Chem. Eng. Sci., **44**, pp. 1539–1545.
[16] Glicksman, L., 1994, *Heat Transfer in Foams—Low Density Cellular Plastics*, N. C. Hilyard and A. Cunningham, eds., Chapman and Hall, London.
[17] Hager, S. L., and Craig, T. A., 1992, "Fatigue Testing of High Performance Flexible Polyurethane Foam," J. Cell. Plast., **28**, pp. 285–303.
[18] Gong, L., and Kyriakides, S., 2005, "Compressive Response of Open Cell Foams Part II: Initiation and Evolution of Crushing," Int. J. Solids Struct., **42**, pp. 1381–1399.
[19] Hilyard, N., and Collier, P., 1987, "A Structural Model Air Flow in Flexible PUR Foams," Chem. Eng. Sci., **6**, pp. 9–26.